
Applied Superconductivity:

Josephson Effect and Superconducting Electronics

**Manuscript to the Lectures during WS 2003/2004, WS 2005/2006, WS 2006/2007,
WS 2007/2008, WS 2008/2009, and WS 2009/2010**

Prof. Dr. Rudolf Gross

and

Dr. Achim Marx

Walther-Meißner-Institut

Bayerische Akademie der Wissenschaften

and

Lehrstuhl für Technische Physik (E23)

Technische Universität München

Walther-Meißner-Strasse 8

D-85748 Garching

Rudolf.Gross@wmi.badw.de

Contents

Preface	xxi
I Foundations of the Josephson Effect	1
1 Macroscopic Quantum Phenomena	3
1.1 The Macroscopic Quantum Model	3
1.1.1 Coherent Phenomena in Superconductivity	3
1.1.2 Macroscopic Quantum Currents in Superconductors	12
1.1.3 The London Equations	18
1.2 Flux Quantization	24
1.2.1 Flux and Fluxoid Quantization	26
1.2.2 Experimental Proof of Flux Quantization	28
1.2.3 Additional Topic: Rotating Superconductor	30
1.3 Josephson Effect	32
1.3.1 The Josephson Equations	33
1.3.2 Josephson Tunneling	37
2 JJs: The Zero Voltage State	43
2.1 Basic Properties of Lumped Josephson Junctions	44
2.1.1 The Lumped Josephson Junction	44
2.1.2 The Josephson Coupling Energy	45
2.1.3 The Superconducting State	47
2.1.4 The Josephson Inductance	49
2.1.5 Mechanical Analogs	49
2.2 Short Josephson Junctions	50
2.2.1 Quantum Interference Effects – Short Josephson Junction in an Applied Magnetic Field	50

2.2.2	The Fraunhofer Diffraction Pattern	54
2.2.3	Determination of the Maximum Josephson Current Density	58
2.2.4	Additional Topic: Direct Imaging of the Supercurrent Distribution	62
2.2.5	Additional Topic: Short Josephson Junctions: Energy Considerations	63
2.2.6	The Motion of Josephson Vortices	65
2.3	Long Josephson Junctions	68
2.3.1	The Stationary Sine-Gordon Equation	68
2.3.2	The Josephson Vortex	70
2.3.3	Junction Types and Boundary Conditions	73
2.3.4	Additional Topic: Josephson Current Density Distribution and Maximum Josephson Current	79
2.3.5	The Pendulum Analog	84
3	JJs: The Voltage State	89
3.1	The Basic Equation of the Lumped Josephson Junction	90
3.1.1	The Normal Current: Junction Resistance	90
3.1.2	The Displacement Current: Junction Capacitance	92
3.1.3	Characteristic Times and Frequencies	93
3.1.4	The Fluctuation Current	94
3.1.5	The Basic Junction Equation	96
3.2	The Resistively and Capacitively Shunted Junction Model	97
3.2.1	Underdamped and Overdamped Josephson Junctions	100
3.3	Response to Driving Sources	102
3.3.1	Response to a dc Current Source	102
3.3.2	Response to a dc Voltage Source	107
3.3.3	Response to ac Driving Sources	107
3.3.4	Photon-Assisted Tunneling	112
3.4	Additional Topic: Effect of Thermal Fluctuations	115
3.4.1	Underdamped Junctions: Reduction of I_c by Premature Switching	117
3.4.2	Overdamped Junctions: The Ambegaokar-Halperin Theory	118
3.5	Secondary Quantum Macroscopic Effects	122
3.5.1	Quantum Consequences of the Small Junction Capacitance	122

3.5.2	Limiting Cases: The Phase and Charge Regime	125
3.5.3	Coulomb and Flux Blockade	128
3.5.4	Coherent Charge and Phase States	130
3.5.5	Quantum Fluctuations	132
3.5.6	Macroscopic Quantum Tunneling	133
3.6	Voltage State of Extended Josephson Junctions	139
3.6.1	Negligible Screening Effects	139
3.6.2	The Time Dependent Sine-Gordon Equation	140
3.6.3	Solutions of the Time Dependent Sine-Gordon Equation	141
3.6.4	Additional Topic: Resonance Phenomena	144
II	Applications of the Josephson Effect	153
4	SQUIDs	157
4.1	The dc-SQUID	159
4.1.1	The Zero Voltage State	159
4.1.2	The Voltage State	164
4.1.3	Operation and Performance of dc-SQUIDs	168
4.1.4	Practical dc-SQUIDs	172
4.1.5	Read-Out Schemes	176
4.2	Additional Topic: The rf-SQUID	180
4.2.1	The Zero Voltage State	180
4.2.2	Operation and Performance of rf-SQUIDs	182
4.2.3	Practical rf-SQUIDs	186
4.3	Additional Topic: Other SQUID Configurations	188
4.3.1	The DROS	188
4.3.2	The SQIF	189
4.3.3	Cartwheel SQUID	189
4.4	Instruments Based on SQUIDs	191
4.4.1	Magnetometers	192
4.4.2	Gradiometers	194
4.4.3	Susceptometers	196

4.4.4	Voltmeters	197
4.4.5	Radiofrequency Amplifiers	198
4.5	Applications of SQUIDs	200
4.5.1	Biomagnetism	200
4.5.2	Nondestructive Evaluation	204
4.5.3	SQUID Microscopy	206
4.5.4	Gravity Wave Antennas and Gravity Gradiometers	208
4.5.5	Geophysics	210
5	Digital Electronics	215
5.1	Superconductivity and Digital Electronics	216
5.1.1	Historical development	217
5.1.2	Advantages and Disadvantages of Josephson Switching Devices	219
5.2	Voltage State Josephson Logic	222
5.2.1	Operation Principle and Switching Times	222
5.2.2	Power Dissipation	225
5.2.3	Switching Dynamics, Global Clock and Punchthrough	226
5.2.4	Josephson Logic Gates	228
5.2.5	Memory Cells	234
5.2.6	Microprocessors	236
5.2.7	Problems of Josephson Logic Gates	237
5.3	RSFQ Logic	239
5.3.1	Basic Components of RSFQ Circuits	241
5.3.2	Information in RSFQ Circuits	246
5.3.3	Basic Logic Gates	247
5.3.4	Timing and Power Supply	249
5.3.5	Maximum Speed	249
5.3.6	Power Dissipation	250
5.3.7	Prospects of RSFQ	250
5.3.8	Fabrication Technology	253
5.3.9	RSFQ Roadmap	254
5.4	Analog-to-Digital Converters	255
5.4.1	Additional Topic: Foundations of ADCs	256
5.4.2	The Comparator	261
5.4.3	The Aperture Time	263
5.4.4	Different Types of ADCs	264

6 The Josephson Voltage Standard	269
6.1 Voltage Standards	270
6.1.1 Standard Cells and Electrical Standards	270
6.1.2 Quantum Standards for Electrical Units	271
6.2 The Josephson Voltage Standard	274
6.2.1 Underlying Physics	274
6.2.2 Development of the Josephson Voltage Standard	274
6.2.3 Junction and Circuit Parameters for Series Arrays	279
6.3 Programmable Josephson Voltage Standard	281
6.3.1 Pulse Driven Josephson Arrays	283
7 Superconducting Photon and Particle Detectors	285
7.1 Superconducting Microwave Detectors: Heterodyne Receivers	286
7.1.1 Noise Equivalent Power and Noise Temperature	286
7.1.2 Operation Principle of Mixers	287
7.1.3 Noise Temperature of Heterodyne Receivers	290
7.1.4 SIS Quasiparticle Mixers	292
7.1.5 Josephson Mixers	296
7.2 Superconducting Microwave Detectors: Direct Detectors	297
7.2.1 NEP of Direct Detectors	298
7.3 Thermal Detectors	300
7.3.1 Principle of Thermal Detection	300
7.3.2 Bolometers	302
7.3.3 Antenna-Coupled Microbolometers	307
7.4 Superconducting Particle and Single Photon Detectors	314
7.4.1 Thermal Photon and Particle Detectors: Microcalorimeters	314
7.4.2 Superconducting Tunnel Junction Photon and Particle Detectors	318
7.5 Other Detectors	328
8 Microwave Applications	329
8.1 High Frequency Properties of Superconductors	330
8.1.1 The Two-Fluid Model	330
8.1.2 The Surface Impedance	333
8.2 Superconducting Resonators and Filters	336
8.3 Superconducting Microwave Sources	337

9 Superconducting Quantum Bits	339
9.1 Quantum Bits and Quantum Computers	341
9.1.1 Quantum Bits	341
9.1.2 Quantum Computing	343
9.1.3 Quantum Error Correction	346
9.1.4 What are the Problems?	348
9.2 Implementation of Quantum Bits	349
9.3 Why Superconducting Qubits	352
9.3.1 Superconducting Island with Leads	352
 III Anhang	 355
 A The Josephson Equations	 357
 B Imaging of the Maximum Josephson Current Density	 361
 C Numerical Iteration Method for the Calculation of the Josephson Current Distribution	 363
 D Photon Noise	 365
I Power of Blackbody Radiation	365
II Noise Equivalent Power	367
 E Qubits	 369
I What is a quantum bit ?	369
I.1 Single-Qubit Systems	369
I.2 The spin-1/2 system	371
I.3 Two-Qubit Systems	372
II Entanglement	373
III Qubit Operations	375
III.1 Unitarity	375
III.2 Single Qubit Operations	375
III.3 Two Qubit Operations	376
IV Quantum Logic Gates	377
IV.1 Single-Bit Gates	377
IV.2 Two Bit Gates	379
V The No-Cloning Theorem	384
VI Quantum Complexity	385
VII The Density Matrix Representation	385

F Two-Level Systems	389
I Introduction to the Problem	389
I.1 Relation to Spin-1/2 Systems	390
II Static Properties of Two-Level Systems	390
II.1 Eigenstates and Eigenvalues	390
II.2 Interpretation	391
II.3 Quantum Resonance	394
III Dynamic Properties of Two-Level Systems	395
III.1 Time Evolution of the State Vector	395
III.2 The Rabi Formula	395
G The Spin 1/2 System	399
I Experimental Demonstration of Angular Momentum Quantization	399
II Theoretical Description	401
II.1 The Spin Space	401
III Evolution of a Spin 1/2 Particle in a Homogeneous Magnetic Field	402
IV Spin 1/2 Particle in a Rotating Magnetic Field	404
IV.1 Classical Treatment	404
IV.2 Quantum Mechanical Treatment	406
IV.3 Rabi's Formula	407
H Literature	409
I Foundations of Superconductivity	409
I.1 Introduction to Superconductivity	409
I.2 Early Work on Superconductivity and Superfluidity	410
I.3 History of Superconductivity	410
I.4 Weak Superconductivity, Josephson Effect, Flux Structures	410
II Applications of Superconductivity	411
II.1 Electronics, Sensors, Microwave Devices	411
II.2 Power Applications, Magnets, Transportation	412
II.3 Superconducting Materials	412
I SI-Einheiten	413
I Geschichte des SI Systems	413
II Die SI Basiseinheiten	415
III Einige von den SI Einheiten abgeleitete Einheiten	416
IV Vorsätze	418
V Abgeleitete Einheiten und Umrechnungsfaktoren	419

J Physikalische Konstanten**425**

List of Figures

1.1	Meissner-Effect	19
1.2	Current transport and decay of a supercurrent in the Fermi sphere picture	20
1.3	Stationary Quantum States	24
1.4	Flux Quantization in Superconductors	25
1.5	Flux Quantization in a Superconducting Cylinder	27
1.6	Experiment by Doll and Naebauer	29
1.7	Experimental Proof of Flux Quantization	29
1.8	Rotating superconducting cylinder	31
1.9	The Josephson Effect in weakly coupled superconductors	32
1.10	Variation of n_s^* and γ across a Josephson junction	35
1.11	Schematic View of a Josephson Junction	36
1.12	Josephson Tunneling	39
2.1	Lumped Josephson Junction	45
2.2	Coupling Energy and Josephson Current	46
2.3	The Tilted Washboard Potential	48
2.4	Extended Josephson Junction	51
2.5	Magnetic Field Dependence of the Maximum Josephson Current	55
2.6	Josephson Current Distribution in a Small Josephson Junction for Various Applied Magnetic Fields	56
2.7	Spatial Interference of Macroscopic Wave Funktions	57
2.8	The Josephson Vortex	57
2.9	Gaussian Shaped Josephson Junction	59
2.10	Comparison between Measurement of Maximum Josephson Current and Optical Diffraction Experiment	60
2.11	Supercurrent Auto-correlation Function	61
2.12	Magnetic Field Dependence of the Maximum Josephson Current of a YBCO-GBJ	63

2.13 Motion of Josephson Vortices	66
2.14 Magnetic Flux and Current Density Distribution for a Josephson Vortex	70
2.15 Classification of Junction Types: Overlap, Inline and Grain Boundary Junction	74
2.16 Geometry of the Asymmetric Inline Junction	77
2.17 Geometry of Mixed Overlap and Inline Junctions	78
2.18 The Josephson Current Distribution of a Long Inline Junction	80
2.19 The Maximum Josephson Current as a Function of the Junction Length	81
2.20 Magnetic Field Dependence of the Maximum Josephson Current and the Josephson Current Density Distribution in an Overlap Junction	83
2.21 The Maximum Josephson Current as a Function of the Applied Field for Overlap and Inline Junctions	84
 3.1 Current-Voltage Characteristic of a Josephson tunnel junction	91
3.2 Equivalent circuit for a Josephson junction including the normal, displacement and fluctuation current	92
3.3 Equivalent circuit of the Resistively Shunted Junction Model	97
3.4 The Motion of a Particle in the Tilt Washboard Potential	98
3.5 Pendulum analogue of a Josephson junction	99
3.6 The IVCs for Underdamped and Overdamped Josephson Junctions	101
3.7 The time variation of the junction voltage and the Josephson current	103
3.8 The RSJ model current-voltage characteristics	105
3.9 The RCSJ Model IVC at Intermediate Damping	107
3.10 The RCJ Model Circuit for an Applied dc and ac Voltage Source	108
3.11 Overdamped Josephson Junction driven by a dc and ac Voltage Source	110
3.12 Overdamped Josephson junction driven by a dc and ac Current Source	111
3.13 Shapiro steps for under- and overdamped Josephson junction	112
3.14 Photon assisted tunneling	113
3.15 Photon assisted tunneling in SIS Josephson junction	113
3.16 Thermally Activated Phase Slippage	116
3.17 Temperature Dependence of the Thermally Activated Junction Resistance	119
3.18 RSJ Model Current-Voltage Characteristics Including Thermally Activated Phase Slippage	120
3.19 Variation of the Josephson Coupling Energy and the Charging Energy with the Junction Area	124
3.20 Energy diagrams of an isolated Josephson junction	127
3.21 The Coulomb Blockade	128

3.22 The Phase Blockade	129
3.23 The Cooper pair box	131
3.24 Double well potential for the generation of phase superposition states	132
3.25 Macroscopic Quantum Tunneling	134
3.26 Macroscopic Quantum Tunneling at Large Damping	138
3.27 Mechanical analogue for phase dynamics of a long Josephson junction	141
3.28 The Current Voltage Characteristic of an Underdamped Long Josephson Junction	145
3.29 Zero field steps in IVCs of an annular Josephson junction	147
4.1 The dc-SQUID	160
4.2 Maximum Supercurrent versus Applied Magnetic Flux for a dc-SQUID at Weak Screening	162
4.3 Total Flux versus Applied Magnetic Flux for a dc SQUID at $\beta_L > 1$	163
4.4 Current-voltage Characteristics of a dc-SQUID at Negligible Screening	165
4.5 The pendulum analogue of a dc SQUID	167
4.6 Principle of Operation of a dc-SQUID	169
4.7 Energy Resolution of dc-SQUIDs	172
4.8 The Practical dc-SQUID	173
4.9 Geometries for thin film SQUID washers	174
4.10 Flux focusing effect in a $\text{YBa}_2\text{Cu}_3\text{O}_{7-\delta}$ washer	175
4.11 The Washer dc-SQUID	176
4.12 The Flux Modulation Scheme for a dc-SQUID	177
4.13 The Modulation and Feedback Circuit of a dc-SQUID	178
4.14 The rf-SQUID	180
4.15 Total flux versus applied flux for a rf-SQUID	182
4.16 Operation of rf-SQUIDS	183
4.17 Tank voltage versus rf-current for a rf-SQUID	184
4.18 High T_c rf-SQUID	187
4.19 The double relaxation oscillation SQUID (DROS)	188
4.20 The Superconducting Quantum Interference Filter (SQIF)	190
4.21 Input Antenna for SQUIDS	191
4.22 Various types of thin film SQUID magnetometers	193
4.23 Magnetic noise signals	194
4.24 Magnetically shielded room	195
4.25 Various gradiometers configurations	196

4.26 Miniature SQUID Susceptometer	197
4.27 SQUID Radio-frequency Amplifier	198
4.28 Multichannel SQUID Systems	201
4.29 Magnetocardiography	203
4.30 Magnetic field distribution during R peak	204
4.31 SQUID based nondestructive evaluation	205
4.32 Scanning SQUID microscopy	207
4.33 Scanning SQUID microscopy images	208
4.34 Gravity wave antenna	209
4.35 Gravity gradiometer	210
 5.1 Cryotron	217
5.2 Josephson Cryotron	218
5.3 Device performance of Josephson devices	220
5.4 Principle of operation of a Josephson switching device	222
5.5 Output current of a Josephson switching device	224
5.6 Threshold characteristics for a magnetically and directly coupled gate	229
5.7 Three-junction interferometer gate	230
5.8 Current injection device	230
5.9 Josephson Atto Weber Switch (JAWS)	231
5.10 Direct coupled logic (DCL) gate	231
5.11 Resistor coupled logic (RCL) gate	232
5.12 4 junction logic (4JL) gate	232
5.13 Non-destructive readout memory cell	234
5.14 Destructive read-out memory cell	235
5.15 4 bit Josephson microprocessor	237
5.16 Josephson microprocessor	238
5.17 Comparison of latching and non-latching Josephson logic	240
5.18 Generation of SFQ Pulses	242
5.19 dc to SFQ Converter	243
5.20 Basic Elements of RSFQ Circuits	244
5.21 RSFQ memory cell	245
5.22 RSFQ logic	246
5.23 RSFQ OR and AND Gate	247

5.24 RSFQ NOT Gate	248
5.25 RSFQ Shift Register	249
5.26 RSFQ Microprocessor	253
5.27 RSFQ roadmap	254
5.28 Principle of operation of an analog-to-digital converter	256
5.29 Analog-to-Digital Conversion	257
5.30 Semiconductor and Superconductor Comparators	262
5.31 Incremental Quantizer	263
5.32 Flash-type ADC	265
5.33 Counting-type ADC	266
6.1 Weston cell	271
6.2 The metrological triangle for the electrical units	273
6.3 IVC of an underdamped Josephson junction under microwave irradiation	275
6.4 International voltage comparison between 1920 and 2000	276
6.5 One-Volt Josephson junction array	277
6.6 Josephson series array embedded into microwave stripline	278
6.7 Microwave design of Josephson voltage standards	279
6.8 Adjustment of Shapiro steps for a series array Josephson voltage standard	281
6.9 IVC of overdamped Josephson junction with microwave irradiation	282
6.10 Programmable Josephson voltage standard	283
7.1 Block diagram of a heterodyne receiver	288
7.2 Ideal mixer as a switch	288
7.3 Current response of a heterodyne mixer	289
7.4 IVCs and IF output power of SIS mixer	290
7.5 Optimum noise temperature of a SIS quasiparticle mixer	293
7.6 Measured DSB noise temperature of a SIS quasiparticle mixers	294
7.7 High frequency coupling schemes for SIS mixers	295
7.8 Principle of thermal detectors	301
7.9 Operation principle of superconducting transition edge bolometer	302
7.10 Sketch of a HTS bolometer	305
7.11 Specific detectivity of various bolometers	305
7.12 Relaxation processes in a superconductor after energy absorption	307
7.13 Antenna-coupled microbolometer	308

7.14 Schematic illustration of the hot electron bolometer mixer	309
7.15 Hot electron bolometer mixers with different antenna structures	311
7.16 Transition-edge sensors	315
7.17 Transition-edge sensors	317
7.18 Functional principle of a superconducting tunnel junction detector	319
7.19 Circuit diagram of a superconducting tunnel junction detector	319
7.20 Energy resolving power of STJDS	321
7.21 Quasiparticle tunneling in SIS junctions	323
7.22 Quasiparticle trapping in STJDS	326
7.23 STJDS employing lateral quasiparticle trapping	326
7.24 Superconducting tunnel junction x-ray detector	327
 8.1 Equivalent circuit for the two-fluid model	332
8.2 Characteristic frequency regimes for a superconductor	332
8.3 Surface resistance of Nb and Cu	335
 9.1 Konrad Zuse 1945	341
9.2 Representation of a Qubit State as a Vector on the Bloch Sphere	342
9.3 Operational Scheme of a Quantum Computer	344
9.4 Quantum Computing: What's it good for?	345
9.5 Shor, Feynman, Bennett and Deutsch	346
9.6 Qubit Realization by Quantum Mechanical Two level System	349
9.7 Use of Superconductors for Qubits	352
9.8 Superconducting Island with Leads	354
 E.1 The Bloch Sphere S^2	370
E.2 The Spin-1/2 System	371
E.3 Entanglement – an artist's view.	373
E.4 Classical Single-Bit Gate	377
E.5 Quantum NOT Gate	378
E.6 Classical Two Bit Gate	380
E.7 Reversible and Irreversible Logic	380
E.8 Reversible Classical Logic	381
E.9 Reversible XOR (CNOT) and SWAP Gate	382
E.10 The Controlled U Gate	382

E.11	Density Matrix for Pure Single Qubit States	386
E.12	Density Matrix for a Coherent Superposition of Single Qubit States	387
F.1	Energy Levels of a Two-Level System	392
F.2	The Benzene Molecule	394
F.3	Graphical Representation of the Rabi Formula	396
G.1	The Larmor Precession	400
G.2	The Rotating Reference Frame	404
G.3	The Effective Magnetic Field in the Rotating Reference Frame	405
G.4	Rabi's Formula for a Spin 1/2 System	408

List of Tables

5.1	Switching delay and power dissipation for various types of logic gates.	233
5.2	Josephson 4 kbit RAM characteristics (organization: 4096 word \times 1 bit, NEC).	236
5.3	Performance of various logic gates	237
5.4	Possible applications of superconductor digital circuits (source: SCENET 2001).	251
5.5	Performance of various RSFQ based circuits.	252
7.1	Characteristic materials properties of some superconductors	325
8.1	Important high-frequency characteristic of superconducting and normal conducting . . .	334
E.1	Successive measurements on a two-qubit state showing the results <i>A</i> and <i>B</i> with the corresponding probabilities $P(A)$ and $P(B)$ and the remaining state after the measurement. . . .	373

Chapter F

Quantum Mechanical Two-Level Systems

We have seen that quantum bits can be represented by every two-level quantum system. There are numerous cases in physics, which can be in first order approximation treated simply as such kind of system. For example, a system with two states whose energies are close and differ very much from those of all other states of the system can be view as a two-level system. Therefore, we briefly summarize here the basic properties of quantum mechanical two-level systems. In particular we address the effect of an external perturbation as well as an internal interaction on the two states. The general treatment of a two-level system will provide some general and important ideas such as quantum resonance, oscillation between two levels etc..

I Introduction to the Problem

We consider a system with a two-dimensional state space. As an orthonormal basis we choose the system of the two eigenstates $|\phi_1\rangle$ and $|\phi_2\rangle$ (cf. (I.2) and I.3)) of the Hamiltonian \mathcal{H}_0 , whose eigenvalues are E_1 and E_2 , respectively:

$$\mathcal{H}_0|\phi_1\rangle = E_1|\phi_1\rangle \quad (\text{I.1})$$

$$\mathcal{H}_0|\phi_2\rangle = E_2|\phi_2\rangle . \quad (\text{I.2})$$

We further take into account an external perturbation or interactions internal to the system, which are not contained in \mathcal{H}_0 , which is called the unperturbed Hamiltonian. The total Hamiltonian then becomes

$$\mathcal{H} = \mathcal{H}_0 + \mathcal{W} \quad (\text{I.3})$$

with the perturbation or coupling \mathcal{W} . The eigenvalues of \mathcal{H} are denoted by $|\Psi_+\rangle$ and $|\Psi_-\rangle$ with the corresponding eigenvalues E_+ and E_- :

$$\mathcal{H}|\Psi_+\rangle = E_+|\Psi_+\rangle \quad (\text{I.4})$$

$$\mathcal{H}|\Psi_-\rangle = E_-|\Psi_-\rangle . \quad (\text{I.5})$$

For simplicity, we will assume that \mathcal{W} is time-independent. In the basis of $\{|\phi_1\rangle, |\phi_2\rangle\}$ of the unperturbed eigenstates of \mathcal{H}_0 , the perturbation \mathcal{W} is represented by a Hermitian matrix

$$\mathcal{W} = \begin{pmatrix} \mathcal{W}_{11} & \mathcal{W}_{12} \\ \mathcal{W}_{21} & \mathcal{W}_{22} \end{pmatrix} . \quad (\text{I.6})$$

\mathcal{W}_{11} and \mathcal{W}_{22} are real and moreover $\mathcal{W}_{12} = \mathcal{W}_{21}^*$.

In the absence of any perturbation or coupling the possible eigenenergies of the system are E_1 and E_2 and the states $|\phi_1\rangle$ and $|\phi_2\rangle$ are stationary states, i.e. if the system is prepared in one of these states it stays there forever.

We now have to evaluate what happens if we are introducing a finite coupling \mathcal{W} . The consequences of the coupling are the following:

- E_1 and E_2 are no longer the possible eigenstates of the system.

If we are measuring the energy of the system only the two values E_+ and E_- are possible, which generally differ from E_1 and E_2 . Therefore, we first have to calculate the new eigenenergies E_+ and E_- in terms of E_1 and E_2 and the matrix elements \mathcal{W}_{ij} of the coupling \mathcal{W} . That is, we have to study the effect of the coupling on the position of the energy levels.

- $|\phi_1\rangle$ and $|\phi_2\rangle$ are no longer stationary states.

Since $|\phi_1\rangle$ and $|\phi_2\rangle$ are in general no longer eigenstates of the total Hamiltonian \mathcal{H} , they are no longer stationary states. If the system stays in the state $|\phi_1\rangle$ at the time $t = 0$, there is a certain probability $P_{12}(t)$ for finding the system in the state $|\phi_2\rangle$ at time t . That is, \mathcal{W} introduces transitions between the two unperturbed states. This justifies the name “coupling” for \mathcal{W} . The dynamic aspect of the effect of \mathcal{W} is the second problem we have to address.

I.1 Relation to Spin-1/2 Systems

It can be shown that the Hamiltonian \mathcal{H} has the same form as that of a spin 1/2 placed in a static magnetic field \mathbf{B} , whose components B_x , B_y and B_z are expressed in terms of E_1 and E_2 and the matrix elements \mathcal{W}_{ij} . That means that we can associate with every two-level system a spin 1/2 placed in a static field \mathbf{B} and described by a Hamiltonian of identical form. The spin is then called a *fictitious spin*. All results we are deriving in the following can then be interpreted in a simple geometric way in terms of a magnetic moment, Larmor precession and other concepts used for spin 1/2 systems. This geometrical interpretation often helps to get a helpful illustration of what is going on. For a discussion of the spin-1/2-system, see Appendix G.

II Static Properties of Two-Level Systems

II.1 Eigenstates and Eigenvalues

We first write the Hamiltonian \mathcal{H} in the $\{|\phi_1\rangle, |\phi_2\rangle\}$ basis of the unperturbed eigenstates:

$$\mathcal{H} = \begin{pmatrix} \mathcal{H}_0 + \mathcal{W}_{11} & \mathcal{W}_{12} \\ \mathcal{W}_{21} & \mathcal{H}_0 + \mathcal{W}_{22} \end{pmatrix}. \quad (\text{II.7})$$

With $|\Psi\rangle = a|\phi_1\rangle + b|\phi_2\rangle$ we obtain the eigenvalue equation

$$\begin{pmatrix} E_1 + \mathcal{W}_{11} - E & \mathcal{W}_{12} \\ \mathcal{W}_{12}^* & E_2 + \mathcal{W}_{22} - E \end{pmatrix} \begin{pmatrix} a \\ b \end{pmatrix} = 0. \quad (\text{II.8})$$

Upon diagonalization of the matrix we find the eigenvalues

$$E_+ = \frac{1}{2}(E_1 + W_{11} + E_2 + W_{22}) + \frac{1}{2}\sqrt{(E_1 + W_{11} - E_2 - W_{22})^2 + 4|W_{12}|^2} \quad (\text{II.9})$$

$$E_- = \frac{1}{2}(E_1 + W_{11} + E_2 + W_{22}) - \frac{1}{2}\sqrt{(E_1 + W_{11} - E_2 - W_{22})^2 + 4|W_{12}|^2} . \quad (\text{II.10})$$

We immediately see that E_+ and E_- are identical to E_1 and E_2 for $W = 0$. The corresponding eigenvectors can be written as

$$|\Psi_+\rangle = \cos \frac{\theta}{2} e^{-i\varphi/2} |\phi_1\rangle + \sin \frac{\theta}{2} e^{+i\varphi/2} |\phi_2\rangle \quad (\text{II.11})$$

$$|\Psi_-\rangle = -\sin \frac{\theta}{2} e^{-i\varphi/2} |\phi_1\rangle + \cos \frac{\theta}{2} e^{+i\varphi/2} |\phi_2\rangle , \quad (\text{II.12})$$

where the angle θ and φ are given by

$$\tan \theta = \frac{2|W_{12}|}{E_1 + W_{11} - E_2 - W_{22}} \quad (\text{II.13})$$

$$W_{21} = |W_{21}| e^{i\varphi} . \quad (\text{II.14})$$

II.2 Interpretation

In order to discuss the above results we first will do a graphical representation of the effect of coupling. The most interesting effect of the perturbation \mathcal{W} is the fact that it possesses off-diagonal matrix elements $\mathcal{W}_{12} = \mathcal{W}_{21}^*$. If the off-diagonal terms would vanish, the eigenstates of \mathcal{H} would be the same as those of \mathcal{H}_0 and the new eigenenergies would be $E_1 + W_{11}$ and $E_2 + W_{22}$. Since the diagonal terms of the perturbation are not very interesting, we will assume $W_{11} = W_{22} = 0$ in the following. With this assumption the expression for the eigenenergies simplify to

$$E_+ = \frac{1}{2}(E_1 + E_2) + \frac{1}{2}\sqrt{(E_1 - E_2)^2 + 4|W_{12}|^2} \quad (\text{II.15})$$

$$E_- = \frac{1}{2}(E_1 + E_2) - \frac{1}{2}\sqrt{(E_1 - E_2)^2 + 4|W_{12}|^2} \quad (\text{II.16})$$

with

$$\tan \theta = \frac{2|W_{12}|}{E_1 - E_2} \quad 0 \leq \theta < \pi \quad (\text{II.17})$$

$$W_{12} = |W_{12}| e^{i\varphi} . \quad (\text{II.18})$$

By introducing the two parameters

$$E_m \equiv \frac{1}{2}(E_1 + E_2) \quad (\text{II.19})$$

$$\Delta \equiv \frac{1}{2}(E_1 - E_2) \quad (\text{II.20})$$

we obtain

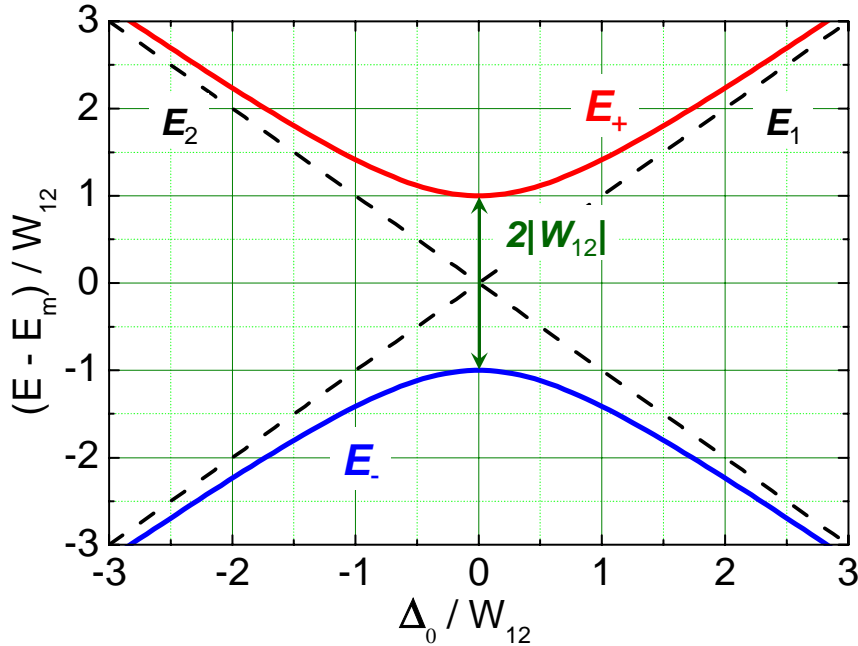


Figure F.1: Variation of the eigenenergies E_+ and E_- as a function of the parameter $\Delta = (E_1 - E_2)/2$. Also shown are the energies E_1 and E_2 (dashed lines).

$$E_+ = E_m + \frac{1}{2} \sqrt{\Delta^2 + 4|W_{12}|^2} \quad (\text{II.21})$$

$$E_- = E_m - \frac{1}{2} \sqrt{\Delta^2 + 4|W_{12}|^2} . \quad (\text{II.22})$$

We see that a variation of E_m corresponds to a shift of the eigenenergies E_+ and E_- along the energy axis. It can be further seen from (F.II.11) to (F.II.14) that the eigenstates $|\Psi_+\rangle$ and $|\Psi_-\rangle$ are not affected by changes of E_m . We therefore are not interested in the effect of E_m . In the following we will set the origin of the energy scale such that $E_m = 0$.

The influence of the parameter Δ is more interesting. In Fig. F.1 we have plotted the variation of the eigenenergies E_+ , E_- , E_1 and E_2 as a function of the parameter $\Delta = (E_1 - E_2)/2$. It is evident that for E_1 and E_2 two straight lines are obtained with slopes +1 and -1, respectively. According to (F.II.21) and (F.II.22), E_+ and E_- describe two branches of a hyperbola, which is symmetrical with respect to the $E = E_m$ and $\Delta = 0$ axis. The asymptotes of the hyperbola are the two straight lines associated with the unperturbed levels. The minimum separation between the two branches is $2|W_{12}|$. We immediately see that $E_+ \rightarrow E_1$ and $E_- \rightarrow E_2$ for $E_1 > E_2$ as well as $E_+ \rightarrow E_2$ and $E_- \rightarrow E_1$ for $E_1 < E_2$.

Discussing the effect of the coupling on the position of the energy levels we see the following: First, in the absence of any coupling the levels (E_1 and E_2) cross at the position ($E = E_m, \Delta = 0$). Under the effect of the off-diagonal coupling the two perturbed levels E_+ and E_- repel each other, i.e. the energy values move further apart from each other, and we obtain the typical ***anti-crossing behavior***. We also see that for any Δ we have

$$|E_+ - E_-| > |E_1 - E_2| . \quad (\text{II.23})$$

This result is well known from other fields of physics. For example, in electronic circuit theory the coupling separates the normal frequencies.

Near the asymptotes we have $|\Delta| \gg |W_{12}|$ and the expressions (F.II.21) and (F.II.22) can be expanded into a power series in $|W_{12}/\Delta|$:

$$E_+ = E_m + \Delta \left(1 + \frac{1}{2} \left| \frac{W_{12}}{\Delta} \right|^2 + \dots \right) \quad (\text{II.24})$$

$$E_- = E_m - \Delta \left(1 + \frac{1}{2} \left| \frac{W_{12}}{\Delta} \right|^2 + \dots \right) . \quad (\text{II.25})$$

On the other hand, for Δ close to zero we obtain

$$E_+ = E_m + |W_{12}| \quad (\text{II.26})$$

$$E_- = E_m - |W_{12}| . \quad (\text{II.27})$$

From this we immediately see that the effect of coupling is more important when the two unperturbed levels have about the same energy. The effect is then of first order as seen from (F.II.26) and (F.II.27), whereas according to (F.II.24) and (F.II.25) it is of second order for $|\Delta| \gg |W_{12}|$.

We next have to discuss the effect of the coupling on the eigenstates. With the parameters E_m and Δ we can rewrite (F.II.17) as

$$\tan \theta = \frac{|W_{12}|}{\Delta} . \quad (\text{II.28})$$

That is, for strong coupling, i.e. $\Delta \ll |W_{12}|$, we have $\theta \simeq \pi/2$. In contrast, for weak coupling, i.e. $\Delta \gg |W_{12}|$, we have $\theta \simeq 0$. Then, at the center of the hyperbola when $E_1 = E_2$, ($\Delta = 0$) we have

$$|\Psi_+\rangle = \frac{1}{\sqrt{2}} \left[e^{-i\varphi/2} |\phi_1\rangle + e^{+i\varphi/2} |\phi_2\rangle \right] \quad (\text{II.29})$$

$$|\Psi_-\rangle = \frac{1}{\sqrt{2}} \left[-e^{-i\varphi/2} |\phi_1\rangle + e^{+i\varphi/2} |\phi_2\rangle \right] . \quad (\text{II.30})$$

Near the asymptotes, when $|\Delta| \gg |W_{12}|$ (weak coupling), we obtain in first order of $|W_{12}|/\Delta$:

$$|\Psi_+\rangle = e^{-i\varphi/2} \left[|\phi_1\rangle + e^{+i\varphi} \frac{|W_{12}|}{2\Delta} |\phi_2\rangle + \dots \right] \quad (\text{II.31})$$

$$|\Psi_-\rangle = e^{+i\varphi/2} \left[|\phi_2\rangle - e^{-i\varphi} \frac{|W_{12}|}{2\Delta} |\phi_1\rangle + \dots \right] . \quad (\text{II.32})$$

As expected, for weak coupling ($\Delta \ll |W_{12}|$) the perturbed states differ only slightly from the unperturbed ones. According to (F.II.31) the state $|\Psi_+\rangle$ differs from $|\phi_1\rangle$ only by the global phase factor $e^{-i\varphi/2}$ with an additional small contribution of the state $|\phi_2\rangle$. According to (F.II.32) the same is true for $|\Psi_-\rangle$. On the other hand, for strong coupling ($\Delta \gg |W_{12}|$) according to (F.II.29) and (F.II.30) the states $|\Psi_+\rangle$ and $|\Psi_-\rangle$ are very different from the unperturbed states $|\phi_1\rangle$ and $|\phi_2\rangle$, since they are linear superpositions of them with coefficients of the same modulus.

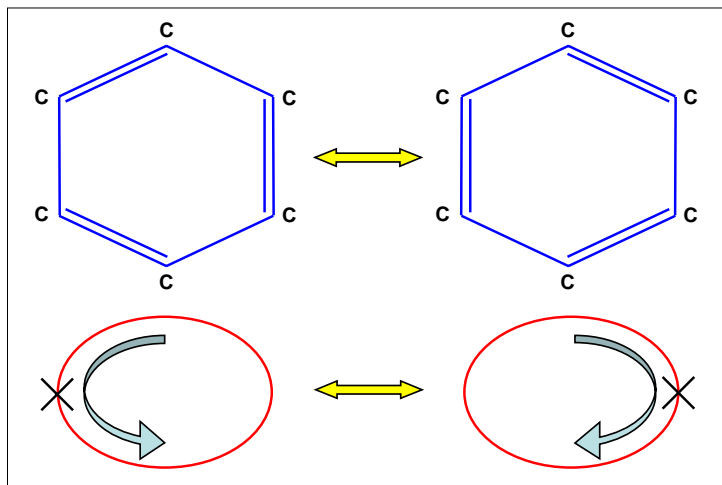


Figure F.2: The two possible configurations of the double bonds in a benzene molecule (top) and of the circulating current in a superconducting loop containing a Josephson junction (bottom).

II.3 Quantum Resonance

We briefly discuss the case where the eigenenergies of \mathcal{H}_0 are two-fold degenerate, i.e. $E_1 = E_2 = E_m$. In this case the coupling W_{12} lifts the degeneracy as discussed above giving rise to a level with reduced energy. That means that if the ground state of a physical system is two-fold degenerate and all other levels are sufficiently far away any purely off-diagonal coupling between the corresponding states is causing a reduction of the ground state energy of the system.

There are many examples of this phenomenon such as the resonance stabilization of the benzene C_6H_6 molecule shown in Fig. F.2. The ground state of the molecule includes three double bonds between neighboring carbons. The eigenfunctions $|\phi_1\rangle$ and $|\phi_2\rangle$ correspond to the two possible configurations of the double bonds shown in Fig. F.2. By symmetry reasons we expect that the ground state energy of the system is $\langle\phi_1|\mathcal{H}|\phi_1\rangle = \langle\phi_2|\mathcal{H}|\phi_2\rangle = E_m$ resulting in a two-fold degenerate ground state. However, the off-diagonal matrix element $\langle\phi_1|\mathcal{H}|\phi_2\rangle$ is not zero resulting in a finite coupling between the states $|\phi_1\rangle$ and $|\phi_2\rangle$. This gives rise to two distinct energy levels with one having an energy lower than E_m . Therefore, the benzene molecule is more stable than we would have expected and the true ground state of the molecule is not represented by one of the two configurations shown in Fig. F.2. The true ground state rather is a superposition of the two configurations.

Further examples are the ionized hydrogen molecule H_2^+ consisting of two protons and one electron. Again there are two possible configurations with the electron localized at proton 1 and proton 2 with degenerate energies. By a finite coupling of these two configurations we again obtain a state with reduced energy. In this state the electron is no longer localized at one of the protons but is delocalized. It is this delocalization which is by reducing the potential energy responsible for the chemical bond.

In chapter 9 as a further example we discuss a superconducting loop with an odd number of Josephson junctions. For half of a flux quantum in the loop there are two degenerate states with circulating currents in opposite directions. Again by a finite coupling a state with lowered energy is achieved given by a superposition of the two configurations.

III Dynamic Properties of Two-Level Systems

III.1 Time Evolution of the State Vector

We assume a state vector at the instant t given by the superposition

$$|\Psi(t)\rangle = a(t)|\phi_1\rangle + b(t)|\phi_2\rangle . \quad (\text{III.33})$$

The evolution of the state vector is determined by the Schrödinger equation

$$i\hbar \frac{d}{dt}|\Psi(t)\rangle = (\mathcal{H}_0 + \mathcal{W})|\Psi(t)\rangle = (\mathcal{H}_0 + \mathcal{W})(a(t)|\phi_1\rangle + b(t)|\phi_2\rangle) . \quad (\text{III.34})$$

By projecting this equation onto the basis vectors $|\phi_1\rangle$ and $|\phi_2\rangle$, we obtain (for $W_{11} = W_{22} = 0$):

$$i\hbar \frac{d}{dt}a(t) = E_1 a(t) + W_{12}b(t) \quad (\text{III.35})$$

$$i\hbar \frac{d}{dt}b(t) = W_{21}a(t) + E_2 b(t) . \quad (\text{III.36})$$

For finite coupling ($|W_{12}| \neq 0$) we obtain a linear system of homogeneous coupled differential equations. In order to solve this system we have to look for the eigenvectors $|\Psi_+\rangle$ with eigenvalue E_+ and $|\Psi_-\rangle$ with eigenvalue E_- of the operator $\mathcal{H} = \mathcal{H}_0 + \mathcal{W}$, whose matrix elements are the coefficients of equations (III.35) and (III.36). We then have to decompose $|\Psi(0)\rangle$ in terms of $|\Psi_+\rangle$ and $|\Psi_-\rangle$ as

$$|\Psi(0)\rangle = \alpha|\Psi_+\rangle + \beta|\Psi_-\rangle , \quad (\text{III.37})$$

where α and β are determined by the initial conditions. We then have

$$|\Psi(t)\rangle = \alpha e^{-iE_+t/\hbar}|\Psi_+\rangle + \beta e^{-iE_-t/\hbar}|\Psi_-\rangle , \quad (\text{III.38})$$

which enables us to derive $a(t)$ and $b(t)$ by projecting $|\Psi(t)\rangle$ onto the basis states $|\phi_1\rangle$ and $|\phi_2\rangle$.

It can be shown that a system with the basis state given by (III.38) oscillates between the two unperturbed states $|\phi_1\rangle$ and $|\phi_2\rangle$. To demonstrate that we assume that $|\Psi(0)\rangle = |\phi_1\rangle$ and calculate the probability $P_{12}(t)$ of finding the system in the basis state $|\phi_2\rangle$ at the time t .

III.2 The Rabi Formula

We first express the state $|\Psi(0)\rangle = |\phi_1\rangle$ on the $\{|\Psi_+\rangle, |\Psi_-\rangle\}$ basis. By inverting the expressions (II.11) and (II.12) we obtain

$$|\Psi(0)\rangle = |\phi_1\rangle = e^{+i\varphi/2} \left[\cos \frac{\theta}{2} |\Psi_+\rangle - \sin \frac{\theta}{2} |\Psi_-\rangle \right] . \quad (\text{III.39})$$

Using the time evolution (III.38) we then obtain

$$|\Psi(t)\rangle = e^{+i\varphi/2} \left[\cos \frac{\theta}{2} e^{-iE_+t/\hbar} |\Psi_+\rangle - \sin \frac{\theta}{2} e^{-iE_-t/\hbar} |\Psi_-\rangle \right] . \quad (\text{III.40})$$

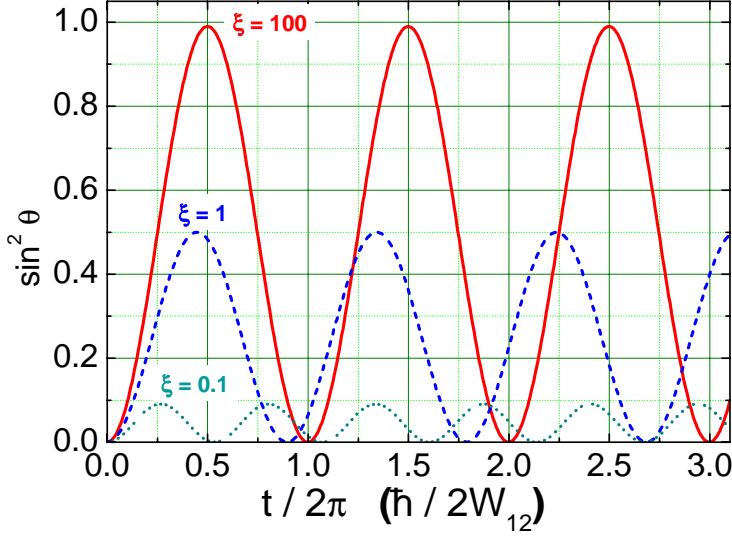


Figure F.3: Variation of the probability P_{12} of finding the system in state $|\phi_2\rangle$ at time t , when it was in state $|\phi_1\rangle$ at $t=0$. $P_{12}(t)$ is shown for three different values of the parameter $\xi = |W_{12}|^2/(E_1 - E_2)^2$ (weak coupling: $\xi \ll 1$, strong coupling: $\xi \gg 1$).

The probability amplitude of finding the system in state $|\phi_2\rangle$ at time t is given by

$$\begin{aligned}\langle \phi_2 | \Psi(t) \rangle &= e^{+i\varphi/2} \left[\cos \frac{\theta}{2} e^{-iE_+ t/\hbar} \langle \phi_2 | \Psi_+ \rangle - \sin \frac{\theta}{2} e^{-iE_- t/\hbar} \langle \phi_2 | \Psi_- \rangle \right] \\ &= e^{+i\varphi/2} \sin \frac{\theta}{2} \cos \frac{\theta}{2} \left[e^{-iE_+ t/\hbar} - e^{-iE_- t/\hbar} \right].\end{aligned}\quad (\text{III.41})$$

With this expression we obtain

$$\begin{aligned}P_{12}(t) &= |\langle \phi_2 | \Psi(t) \rangle|^2 = \frac{1}{2} \sin^2 \theta \left[1 - \cos \left(\frac{E_+ - E_-}{\hbar} t \right) \right] \\ &= \sin^2 \theta \sin^2 \left(\frac{E_+ - E_-}{2\hbar} t \right).\end{aligned}\quad (\text{III.42})$$

Using the expression (F.II.15) and (F.II.16) for E_+ and E_- we can rewrite this equation to obtain the so called **Rabi formula**

$$P_{12}(t) = \frac{2|W_{12}|^2}{4|W_{12}|^2 + (E_1 - E_2)^2} \sin^2 \left[\sqrt{4|W_{12}|^2 + (E_1 - E_2)^2} \frac{t}{2\hbar} \right]. \quad (\text{III.43})$$

We see from (F.III.42) and (F.III.43) that $P_{12}(t)$ oscillates with the frequency $(E_+ - E_-)/\hbar$, which is the Bohr frequency of the system. We further see that $P_{12}(t)$ varies between zero and a maximum value equal to $\sin^2 \theta$, which is obtained for the times $t = (2n+1)\pi\hbar/(E_+ - E_-)$ with $n = 0, 1, 2, 3, \dots$ (see Fig. F.3). According to (F.III.43) the value of $\sin^2 \theta$ as well as the oscillation frequency are functions of $|W_{12}|$ and $(E_1 - E_2)$.

For $E_1 = E_2$ we have $(E_+ - E_-)/\hbar = 2|W_{12}|/\hbar$. Then, according to (F.III.43) $P_{12}(t)$ has the maximum possible value of unity at the moments $t = (2n+1)\pi\hbar/2|W_{12}|$. That is, the system that is originally in the state $|\phi_1\rangle$ at $t = 0$ is in the state $|\phi_2\rangle$ at $t = \pi\hbar/2|W_{12}|$. Evidently any coupling between two states of equal

energy causes the system to oscillate completely between the two states at a frequency proportional to the coupling. This phenomenon is known also for classical systems. For example, when we couple two pendulums of the same frequency by suspending them from the same support and we set only pendulum 1 into motion at $t = 0$, we will have after a certain time pendulum 1 in complete rest whereas pendulum 2 is oscillating with the initial amplitude of pendulum 1.

Fig. F.3 shows that the oscillation period $(E_+ - E_-)/\hbar$ of $P_{12}(t)$ decreases when $(E_1 - E_2)$ increases due to a decrease of the parameter $\xi = |W_{12}|^2/(E_1 - E_2)^2$ at constant $|W_{12}|$. Note that for weak coupling ($|W_{12}| \ll E_1 - E_2$) we have $\xi \ll 1$ and hence $\sin^2 \theta$ becomes very small. This is not surprising, since in the case of weak coupling the state $|\phi_1\rangle$ is very close to the stationary state $\Psi_+\rangle$ and therefore the system starting at state $|\phi_1\rangle$ evolves very little over time.

Above we have mentioned the H_2^+ molecule as an example for a two-level system. According to the result (F.III.43) we expect an oscillation of the electron between the two protons of the molecule at a frequency given by the Bohr frequency $(E_+ - E_-)/\hbar$ given by the two stationary states $\Psi_+\rangle$ and $\Psi_-\rangle$ of the molecule. This oscillation corresponds to an oscillation of the mean value of the electric dipole moment of the molecule. Therefore, when the molecule is not in a stationary state, an oscillating dipole field can appear. Such an oscillating dipole can exchange energy with an electromagnetic field of the same frequency. Hence, this frequency must be seen in the absorption and emission spectrum of the molecule. Of course, the same is true for a superconducting flux or charge qubit representing a two-level system. In many experiments the interaction of an electromagnetic field of varying frequency with the qubit has been measured showing absorption/emission features at the characteristic frequency $(E_+ - E_-)/\hbar$.